Investigation of Fe isotope systematics for the complete sequence of natural and metallurgical processes of Ni lateritic ores: Implications for environmental source tracing

Gildas Ratié, Jérémie Garnier, Lucieth Cruz Vieira, Daniel Araújo, Michael Komárek, Franck Poitrasson, Cécile Quantin

Investigation of Fe isotope systematics for the complete sequence of natural and metallurgical processes of Ni lateritic ores: Implications for environmental source tracing

Gildas Ratié[1], Jérémie Garnier[2], Lucieth Cruz Vieira[2], Daniel F. Araújo[3], Michael Komárek[1], Franck Poitrasson[4], Cécile Quantin[5]

Graphical abstract

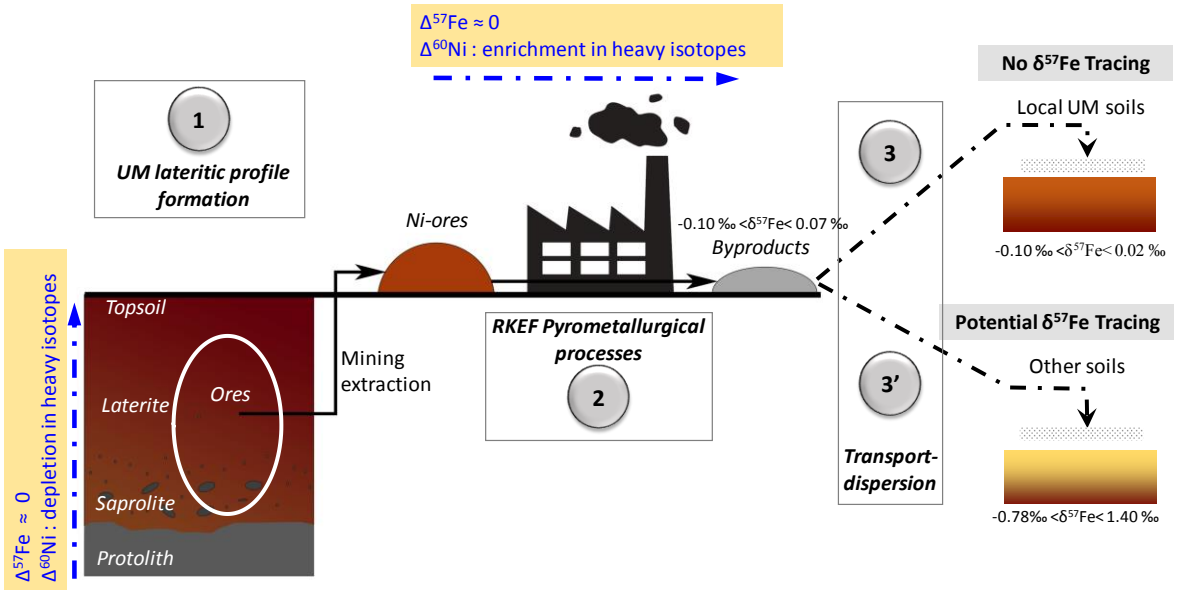

Investigation of Fe isotope systematics for the complete sequence of natural and metallurgical processes of Ni lateritic ores: Implications for environmental source tracing

Gildas Ratié[1], Jérémie Garnier[2], Lucieth Cruz Vieira[2], Daniel F. Araújo[3], Michael Komárek[1], Franck Poitrasson[4], Cécile Quantin[5]

Highlights

- Fe mobility does not induce isotopic fractionation during chemical weathering.
- There is no evidence of Fe isotope fractionation during the RKEF smelting process.
- Smelting slags are stamped with δ^{57}Fe values from Ni laterite ores.
- The use of Fe isotopes as an environmental tracer in lateritic soils is limited.
- Fe isotopes may be potential tracer of mining activities in non-lateritic soils.

Investigation of Fe isotope systematics for the complete sequence of natural and metallurgical processes of Ni lateritic ores: Implications for environmental source tracing

Gildas Ratié[1*], Jérémie Garnier[2], Lucieth Cruz Vieira[2], Daniel F. Araújo[3], Michael Komárek[1], Franck Poitrasson[4], Cécile Quantin[5]

[1]*Department of Environmental Geosciences, Faculty of Environmental Sciences, Czech University of Life Sciences Prague, Kamýcká 129, 165 00, Prague - Suchdol, Czech Republic*

[2]*UnB, IG/GMP-ICC Centro, Campus Universitário Darcy Ribeiro, 70910-970, Brasilia-DF, Brazil/Laboratoire Mixte International "Observatoire des Changements Environnementaux" (LMI OCE), Institut de Recherche pour le Développement/University of Brasilia, Campus Darcy Ribeiro, Brasilia, Brazil*

[3]*Laboratoire de Biogéochimie des Contaminants Métalliques, Ifremer, Centre Atlantique, F44311 Nantes Cedex 3, France*

[4]*Laboratoire Géosciences Environnement Toulouse, UMR 5563 CNRS-UPS-IRD-CNES, 14-16, avenue Edouard Belin, 31400, Toulouse, France.*

[5]*UMR 8148 GEOPS, Université Paris-Saclay – CNRS, 91405 Cedex, France.*

*corresponding author: ratie@fzp.czu.cz

Keywords

- metal cycle
- chemical weathering
- smelting
- byproducts

Abstract

Metal isotopes are versatile pollutant source trackers, but biogeochemical processes can overprint or alter the original source isotopic fingerprint and thus hinder contamination tracing. Here, we explore Fe isotope systematics for the complete range of natural and metallurgical processes related to Ni lateritic ores from Barro Alto, Brazil, to assess its potential as tracer in polluted lateritic soil contexts developed in an ultramafic system.

The homogeneous $\delta^{57}Fe$ values from protolith to soil confirmed that no significant Fe isotopic variation occurred during the formation of the deep lateritic profile. In addition, no Fe isotopic fractionation was found during the smelting process. Although the $\delta^{57}Fe$ values resulting from mining activities fall within the range of terrestrial sample signatures, the conservation of the $\delta^{57}Fe$ values from the ores to the byproducts is an advantage for tracing anthropogenic sources when (i) the pyrometallurgical plant uses feeding material with Fe ores imported from other geological formations exhibiting different $\delta^{57}Fe$ values and/or (ii) the byproducts are transported or dispersed to other locations with different $\delta^{57}Fe$ signatures in the topsoil.

1. Introduction

The increasing global demand for metals has led to intense mining activities and their consequent remobilization and enrichment in surface compartments, notably soils (Nriagu and Pacyna, 1988; Rauch and Pacyna, 2009). Of particular concern is the soil contamination associated with metal extraction from saprolite ores such as the extraction of Ni, where its concentration of approximately 3 wt% implies high economic value (Butt and Cluzel, 2013). However, in recent decades, limonitic ore refining has increased as a result of the application of modern technologies (allowing better yield recovery). In that ore, Fe contents can reach 40 wt% and Ni can occur in concentrations of up to 1 wt% in Fe oxides (primarily hematite and goethite) (Manceau et al., 2000; Quantin et al., 2002; Dublet et al., 2012 and 2015, Ratié et al., 2018). Smelting processes such as the rotary kiln-electric furnace (RKEF) process are used to extract Ni from mixtures of saprolite and limonite ores, yielding crude ferronickel (FeNi) composed of approximately 70%

Fe and 30% Ni (Crundwell et al., 2011). In the feeding material, Fe is primarily present as Fe(III) in Fe oxides and Fe(II)/Fe(III) in the saprolite (e.g., smectite-type, serpentine, pyroxene, spinel, olivine, etc.). The byproducts of the ore refining process, i.e., fly ash and slag wastes, are Si-, Fe- and Mg-rich materials.

Generally, the pyrometallurgical wastes are either stored in the surrounding environment in settling ponds (fly ash), dumped (slags) or partially reprocessed for metal recovery (fly ash). Such disposal sites are susceptible to rainfall leaching and wind remobilization that can lead to the contamination of the superficial environment and pose major risks to public health (Ettler et al., 2018). The release of metals in soils by leaching is highly time-dependent (Barna et al., 2004; Bril et al., 2008; Seignez et al., 2008; Ettler and Johan, 2014) and increases when slag disposal sites are flooded and/or occurs in water-saturated environments (Ganne et al., 2006; Navarro et al., 2008; Houben et al., 2013). Thus, understanding the dynamics of metals at contaminated sites, i.e., their sources, pathways and sinks is of the highest priority to develop effective environmental management and monitoring programs.

To that purpose, the use of metal isotopic signatures can be useful in the identification and quantification of contaminant sources and for understanding how biogeochemical processes affect contaminant transport (Bullen, 2014; Wiederhold, 2015). The primary challenge to successfully applying isotopes as environmental tracers is to identify isotopic signatures that are distinctive between anthropogenic and natural materials and to deconvolve the original isotopic signal from subsequent isotopic fractionations induced by biogeochemical processes. In the case of stable isotopes of Zn and Cd, industrial or metallurgical fractionation during ore refining results in manufactured products and byproducts that are isotopically distinct from their natural sources (e.g., Mattielli et al., 2006; Kavner et al., 2008; Sivry et al., 2008; Sonke et al., 2008; Shiel et al., 2010; Chrastný et al., 2016; Klein and Rose, 2020). In contrast, Cu and Ni show little or no stable isotope fractionation during ore refining by smelting due to their high boiling points (Bigalke et al., 2010; Ratié et al., 2016). As a consequence, the manufactured metals, slags and other metallurgical byproducts have an isotopic signature similar to that of the ore concentrates. In soil pollution contexts, overlaps between ore and natural background isotope compositions may compromise source

tracking (Ratié et al., 2016; Šillerová et al., 2017). To overcome this drawback, the coupling of two stable metal isotope systems has been used to enhance source discrimination and deconvolution of the different biogeochemical processes involved in acid-mine mining (Borrok et al., 2009), coastal systems (Araújo et al., 2019a, b) and urban atmospheres (Souto-oliveira et al., 2017, 2018).

In this work, we explore Fe isotope systematics in lateritic soils from an ultramafic system and the associated Ni ores refined in a pyrometallurgical system in Barro Alto, Brazil. Previously, an analogous study was conducted to investigate Ni isotopes, which demonstrated a low level of Ni isotope fractionation during ore refining that did not allow the use of Ni isotopes as tracers of contamination (Ratié et al., 2016). Here, we attempt to gain new insights by using Fe isotopes which have never been explored in this context despite their potential.

Iron isotopes demonstrate special features of fractionation, both abiotically and biotically induced in natural and anthropic materials, that can be useful in our case study (Dauphas et al., 2017; Wu et al., 2019). As demonstrated by Poitrasson et al. (2008) for chemical weathering in Cameroon, the lateritization process, which occurs over several million years, result in almost no δ^{57}Fe variation. This feature was subsequently confirmed on other laterites from China and the Philippines, the latter being developed on peridotites (Liu et al., 2014; Li et al., 2017). In contrast, modern soil studies from both temperate and tropical areas and even Paleoproterozoic laterites showed much greater Fe isotopic variation (Fante and Depaolo, 2004; Emmanuel et al., 2005; Thompson et al., 2007; Wiederhold et al., 2007; Yamaguchi et al., 2007; Fekiacova et al., 2013; Akerman et al., 2014). A key driving factor was the separation of two iron pools having different iron redox states, and therefore contrasted Fe isotope signatures (Wu et al., 2019). Iron isotope systematics was also successfully used to fingerprint anthropogenic and natural sources in river sediments (Chen et al., 2014) in an alpine watershed impacted by acid mine drainage (Borrok et al., 2009; Herbert Jr and Schippers, 2008). Iron isotopes were also used to trace anthropogenic combustion through the collection of aerosols from sources in the Sahara, North America, Europe (Flament et al., 2008; Conway et al., 2019) and Japan (Kurisu et al., 2016). These studies suggest that anthropogenic Fe signatures

originating from metallurgical, industrial and urban activities can display significant differences in Fe isotopes relative to natural sources. However, the understanding of potential fractionation of Fe in ore smelting/refining remains unclear. Only one study has been conducted to date, which examines Fe production by an ancient Galo-Roman bloomery process. The study of a major Roman site of Fe production known as "Les Martys" (Montagne Noire Massif, SW France) showed no significant Fe isotope fractionation from the Roman production of iron bars (Milot et al., 2016). Thus, the present study aims to explore (1) the Fe isotope fractionation associated with Ni-rich laterite ore formation, (2) the Fe isotope fractionation associated with Ni laterite ore smelting and refining during the RKEF processing, and (3) the potential of Fe isotopes to trace the environmental impact of FeNi production.

2. Materials and methods

2.1. Ore deposit and mining contexts

The RKEF process for the production of FeNi was first developed in 1953-1954 and was applied commercially to the treatment of garnieritic ores in New Caledonia. Later, it was adopted by FeNi producers for Ni ore deposits across the globe: the Dominican Republic, Colombia, Venezuela, Indonesia, Japan, etc. (Warner et al., 2006). In recent years, at least three major new FeNi smelters have been constructed and are in operation: Barro Alto and Onça Puma in Brazil and Koniambo in New Caledonia (Oxley et al., 2016). The Ni deposits of Barro Alto, located in the midwestern region of Goiás (in Central Brazil), constitute a large Ni reserve that is exploited by the Anglo American company using open pits.

The metallurgical plant at Barro Alto uses the RKEF process to produce FeNi from a nominal 2.4 Mt/y of ore. Its production has increased nearly 2-fold since 2011 to 43 kt of total Ni output in 2018 (Anglo American PLC Annual Report, 2012 and 2018). The deposit, with the ore reserves estimated in 2018 at 52 Mt containing 586 kt of Ni (Anglo American PLC Annual Report, 2018) is in the Barro Alto mafic-ultramafic complex that is part of the Pre-Cambrian shield. This ultramafic complex is composed of

serpentinized dunites, pyroxenites and gabbros (Ferreira Filho et al., 2010). The mineralization corresponds to the surficial weathered portions of the serpentinites (Butt and Cluzel, 2013).

Four main steps are involved in FeNi production (Crundwell et al., 2011): drying of the ore before its introduction into the rotating kiln; calcination with coal, oil or other organic products within the kiln; reduction in an electric furnace and refining of the molten FeNi in another electric furnace (Fig. 1). These processes generate enormous quantities of byproducts (Dalvi et al., 2004; Warner et al., 2006) containing significant amounts of metals (Ni, Co, Cr, Mn, Fe, etc.) (Ettler et al., 2016).

The fly ash (F) generated contains large amounts of Fe and Ni and is recovered by electrostatic filters. The collected fly ash is then recycled into the calcination kiln (Fig. 1). The smelting slags (SS) are composed of high temperature silicates, amorphous glass as well as inclusions of small FeNi metallic particles (Ettler et al., 2016). They are dumped and stored near the plant. The molten FeNi is then refined through a two-step process that produces two types of refining slags: black refining slag (BRS) and white refining slag (WRS) after the removal of P and S, respectively. The FeNi is produced in the form of small ingots or water-granulated "beans".

2.2. Samples

The list of samples is detailed in Table 1. The sampling for Fe isotope determinations included natural samples from soils and lateritic profiles in the Barro Alto ultramafic region and materials used and produced during the RKEF processes. The latter included the Ni ores employed as feeding material (n=2), the smelting slags (SS, n=2), white and black refining slags (WRS and BRS, n=2) and the final manufactured FeNi ingot (n=1). As previously mentioned, the fly ash is reinjected in the calcination step.

A 28 m deep lateritic profile drilled by the Anglo American company were obtained at intervals of 1 m, labeled "RC", was used for this study (Ratié et al., 2018). As the overburden (0-3 m) was removed to facilitate drilling by the mining company, the core/profile starts at the depth of 3 m. To complete the profile, a soil in the vicinity was collected at three different depths: 0-10 cm (BAS1 0-10) or topsoil, 10-30 cm (BAS1 10-30) and 30-80 cm (BAS1 30-80) (Ratié et al., 2015). Five lateritic samples of the RC profile (RC

0-1, RC 6-7, RC 16-17, RC 24-25, and RC 27-28) were selected for Fe isotope characterization. RC 0-1 was defined as the top of the lateritic profile. RC 6-7 was the part of the lateritic profile dominated by Fe oxides. RC 16-17 was the smectitic horizon exhibiting high Ni content, and RC 24-25 was a characteristic saprolitic sample rich in serpentine and exhibiting a relatively low Fe content. RC 27-28 was the deepest sample, mainly composed of primary minerals (olivine) and was considered the protolith. The sample selection strategy involved the sampling of a weathering gradient of the ultramafic parent rock.

2.3. Sample preparation and Fe chemical separation

All the samples were homogenized and finely crushed, and approximately 100 mg of the samples was aliquoted to Savillex vessels. The samples were then digested on a hot plate using a multiple-step acid procedure with HF, HNO3, and HCl. First, an acid mixture of 5 mL of concentrated HF and 1.5 mL of $HClO_4$ at 180°C was added until evaporation was complete. Subsequently, a mixture of concentrated HCl-HNO_3 (3.75 mL and 1.25 mL, respectively) at 150°C was added and evaporated to dryness. Finally, the samples were dissolved in an acid medium of 6 M HCl and split into aliquots for elemental and isotopic determinations. For this step, the sample solution aliquots were processed through chromatographic columns for chemical separation prior to isotope analysis. The iron was purified using Bio Rad AG1 X4 (200–400 mesh) anionic resin loaded into thermo-retractable Teflon columns for exchange chromatography in an HCl medium as described by Poitrasson et al. (2004). Blank levels of the chemical procedure reached ~4 ng of Fe, which is negligible for the sample preparation process. All of the reagents were of analytical grade or bidistilled and the sample preparation for isotope analysis was conducted in the clean laboratories of GEOPS (Université Paris Saclay, France).

2.4. Iron isotope composition measurements

Iron isotope measurements were performed at the GET laboratory (Toulouse, France) using the Observatoire Midi-Pyrénées ICP facility in high or medium mass resolution mode on a Thermo Electron

Neptune MC ICP MS. The Fe isotopic ratios were determined following the procedure detailed by Poitrasson and Freydier (2005).

This method involved a mass bias correction using a combination of the "standard-sample bracketing" approach using IRMM-14 as the Fe standard and Ni doping of the purified Fe samples. This approach accurately corrected for mass bias deviations due to residual matrix effects. The Fe isotope compositions were expressed in the delta notation relative to the European reference material IRMM-14 as follows:

$$\delta^{57}Fe = \left(\frac{\left(\frac{^{57}Fe}{^{54}Fe}\right)_{sample}}{\left(\frac{^{57}Fe}{^{54}Fe}\right)_{IRMM-14}} - 1 \right) \times 1000 \quad \text{(Eq. 1)}.$$

The GET in-house hematite standard from Milhas (Pyrénées, France) was measured every 6 samples. The long-term external reproducibility of the method was estimated from replicate analyses of this standard in every session. In this work, the mean δ^{57}Fe value of individual measurements for hematite was 0.762 ± 0.083 ‰ (2 SD, n=21) in the GET laboratory, whereas data pooled in groups of 3 (which is the minimum number of times each sample should normally be analyzed) yielded a δ^{57}Fe = 0.764 ± 0.057 ‰ (2 SD, n=7). These values are consistent with those from previous measurements conducted for over three years in the same analytical sequences and performed in various laboratories (Poitrasson et al., 2014). Variation in the δ^{57}Fe reported for the samples in this study is expressed as two standard errors (2 SE) of the mean (n=3).

3. Results and discussion

3.1. Bulk compositions

The mineralogy and chemical composition of the entire set of samples are discussed in detail in Ratié et al. (2015, 2016) and Ettler et al. (2016). The weathered material derived from the ultramafic rocks is strongly depleted in Mg and enriched in Fe from the base to the top of weathering profile. The mineralogy of the weathered profile changes from the base (RC 27-28) to the top (BAS1 0-10, BAS1 10-30, BAS1 30-

80) from the dominance of primary minerals (serpentine, chlorite, amphibole, olivine and traces of quartz) to secondary minerals such as goethite and hematite with some preserved primary minerals such as chromite.

Based on the overall sampling from Ratié et al. (2016), the industrial plant feeding material, i.e., the ore, exhibits high Fe and Mg contents of 118-178 g kg^{-1} and 81.4-110 g kg^{-1}, respectively, whereas nickel content ranges from 16.9 to 23.2 g kg^{-1}. Iron and Mg contents of the smelting slags (SS) range from 68.8 to 142.7 g kg^{-1} and 153 to 188 g kg^{-1}, respectively, and the Ni concentration is relatively low ($\leq$ 2 g kg^{-1}). According to a previous study of these smelting wastes (Ettler et al., 2016), more than 95% of the total Fe occurs as Fe(II) in the smelting slag, whereas 80% of the total Fe in the reinjected fly ash is present as Fe(III). The refined slags (WRS and BRS) are richer in Fe (71.2-179 g kg^{-1}) compared with smelting slags. Ferronickel is composed of roughly two-thirds Fe (66-69 wt%) and one-third Ni (31-34 wt%).

The Anglo American plant uses 2.4 Mt/y of Ni ore to produce 41,000 t/y of Ni as FeNi (Moore, 2012 and personal communications). The quantity of Ni introduced in the process, as calculated using an ore Ni content of 1.96 ± 0.23 wt%, is 47,000 ± 5,400 t/y. This led to a production yield of nearly 88 ± 10% Ni for the 2016 production (Anglo American PLC Annual Report, 2017). For Fe, given the mean Fe content in ore of 15.1 wt% and a production of 41,000 t of FeNi, 362,400 t of Fe were processed and 82,000 t of Fe were produced as FeNi with almost 80% of the initial Fe remaining in the waste. The difference between the incoming Fe/Ni and FeNi production corresponds to the residual Fe/Ni in the different waste materials.

3.2. Iron isotope compositions

3.2.1. Ultramafic rocks weathering

Based on mantle-derived and crustal igneous rocks, the bulk silicate Earth shows a homogenous Fe isotopic signature of approximately $\delta^{57}Fe = 0.10 \pm 0.03$ ‰ (Poitrasson and Freydier, 2005; Poitrasson, 2006; Johnson and Beard, 2006). In Barro Alto, the deepest sample from the profile (RC 27-28), which contains the typical mineral assembly of serpentinized ultramafic rocks, was determined to be the least weathered sample and thus it was considered representative of the protolith material (Ratié et al., 2018). The base of the weathering profile (0.08 ± 0.20 ‰) is consistent with the bulk silicate Earth value (Poitrasson, 2006).

The $\delta^{57}Fe$ values of the weathered materials range from -0.10 ± 0.07 ‰ (BAS1 0-10) to 0.07 ± 0.05 ‰ (RC 0-1) and fall within the range of values reported in the literature for soils (Wu et al., 2019). Given the level of analytical variation (2 SE), these results show no significant isotopic differences in $\delta^{57}Fe$ values between the protolith and the weathered materials, similarly to other lateritic profiles elsewhere. (Cameroon, Poitrasson et al., 2008) (China, Liu et al., 2014; Philippines, Li et al., 2017).

The gain and loss of Fe during chemical weathering can be evaluated by the calculation of the enrichment factor "τ_{Fe}" (Table 1). A negative value for τ_{Fe} reflects a true loss in Fe from the weathered material compared with the protolith, and a positive value indicates a gain in Fe. If τ_{Fe} is 0, Fe is considered immobile during weathering with respect to the regolith. The entire Barro Alto profile displays τ_{Fe} values ranging from -0.10 to 0.22, which suggests that Fe shows little mobility from all of the layers of the profile (Table 1, Fig. 2). However, a caveat is that this inference does not consider possible soil density changes that were not measured in this study. The topography of the complex is characterized by a succession of hills and valleys with altitudes ranging from 750 m to 1100 m dominating the large plain (De Oliveira et al., 1992). As a consequence, the weathering conditions occurring on the complex are considered as well drained. In the tropical condition, from the base to the top of the profile, olivine and serpentine are replaced by Fe-oxides and Mg silicates through a series of transitional phyllosilicates (Colin et al. 1990; Butt and Cluzel, 2013). In addition, the bulk Fe isotopic composition remains homogeneous along the lateritic profile (-0.10 ‰ to 0.08 ‰), indicating that the $\delta^{57}Fe$ values were not significantly altered by the loss or gain of Fe during chemical weathering (Fig 2). These features agree with the oxidative conditions along the lateritic profile and the high rate of lixiviation. Therefore, the formation of secondary Fe-bearing phases plays a minor role in fractionating Fe isotope during ultramafic rock weathering. This result is (i) consistent with those obtained from weathering profiles in Cameroon (Poitrasson et al., 2008), China (Liu et al., 2014) and the Philippines (Li et al., 2017) under tropical conditions

In contrast, in the case of Ni, weathering was associated with isotopic fractionation as part of the Ni was leached, leading to a weathering profile that was depleted in heavy Ni isotopes. This depletion of heavy

Ni isotopes was interpreted as the preferential sorption and incorporation of light Ni isotopes into Fe oxides (Wasylenki et al., 2015) and phyllosilicates (type 2:1) (Ratié et al., 2018) in addition to Ni isotopic fractionation during the first stage of weathering, i.e., during mineral dissolution (Ratié et al., 2015, 2018).

3.2.2. Metallurgical production

The Fe isotopic composition of the metallurgical samples ranges from -0.10 ± 0.09 ‰ (smelting slags) to 0.07 ± 0.12 ‰ (FeNi). The Fe isotope compositions are analytically indistinguishable from the feeding materials to the final FeNi product (Fig. 3). Although the process yields for Fe are very low (22%), the isotope composition is homogeneous in all byproducts. Given the high-temperature natural processes that occur in the Earth's core and the differentiation in an early silicate magma ocean, it seems logical that there is not significant Fe isotope fractionation in the FeNi alloy and the ultramafic silicate melt (Poitrasson et al., 2009). Within the 2-7.7 GPa pressures, the chemical and Fe isotope equilibrium was reached at 2,000°C within 100 s ($\Delta^{57}Fe_{metal\text{-}silicate\ glass}$= 0.047 ± 0.063 ‰). The high temperature conditions found in the electric furnace at 1,600°C could induce a similar rapid equilibrium and hence inhibit detectable Fe isotopic fractionation between FeNi and the feeding material.

In the furnace, metal isotope fractionation is dependent on the relative isotope mass difference, the viscosity of the alloy, the mass of the matrix atoms and the temperature range (Ott, 1969; Lodding et al., 1970; Ginoza and March, 1985). In the RKEF processes, the smelting temperature (1,600°C) is very close to the Fe fusion point (1,538°C), and the homogeneous $\delta^{57}Fe$ value in the metallurgical wastes argues for an absence of the thermal gradients responsible for possible metal stable isotope fractionation. In fact, in modern enhanced industrial processes such as RKEF, the Fe distribution is homogeneous at the molten scale during the different steps. This inference is supported by experiments reproducing the ancient bloomery process at 1,300°C, which shows no significant Fe isotopic heterogeneity within the Fe metal products, although they did not go beyond the pasty state at such low temperatures (Milot et al., 2016).

3.2.3. Implications for environmental tracing

Our study shows that the anthropogenic $\delta^{57}Fe$ values fall within the range of the raw material signatures in Barro Alto that include the Earth's mean Fe isotopic composition, in a manner similar to that of the Ni isotope systematics previously investigated (Fig. 3). Such an outcome hinders the use of Fe isotopes as an environmental tracer in the context of soils impacted by metallurgical activity if the raw material comes from the same locality, which is the case at Barro Alto.

However, the conservation of the $\delta^{57}Fe$ values from the feeding material to the metallurgical wastes can be advantageous to trace anthropogenic sources in cases (i) where pyrometallurgical plants use feeding material imported from another deposit exhibiting $\delta^{57}Fe$ values that are distinct from local environment and when (ii) the metallurgical byproducts deposited in open-air undergo redox reactions triggered by changes in the biogeochemical conditions of the surrounding environment. A compilation of published $\delta^{57}Fe$ of ores (Milot et al., 2016, 2018) have noted that the iron isotopic signature exhibits a wide range of values from -2.8 ‰ to 2.4 ‰ for different mineral deposits (sedimentary, hydrothermal, skarn and supergene deposits (e.g., Graham et al., 2004; Markl et al., 2006; Johnson et al., 2008; Fabre et al., 2011; Wang et al., 2011; Cheng et al., 2015; Pi et al., 2015; Wawryk and Foden, 2015; Texeira et al., 2017). Moreover, modern soils from temperate areas (e.g., Fantle and Depaolo, 2004; Emmanuel et al., 2005; Wiederhold et al., 2007; Fekiacova et al., 2013, Wu et al., 2019) and wet tropical soils involving Fe redox cycling (Thompson et al., 2007; Akerman et al., 2014) yield $\delta^{57}Fe$ ranges of -0.9 ‰ to 1.4 ‰. This range represents significant variations relative to the natural $\delta^{57}Fe$ values in Barro Alto soils, which range from -0.10 ‰ to 0.02 ‰ only. This therefore permits the use Fe isotopes to trace contamination when raw materials from other locations are employed, as long as they are not regular lateritic soils. Therefore, the use of a different feeding material for the industrial plant at the Barro Alto site would allow tracing of the anthropogenic input to the local environment. In this case, Fe isotopes could be a better tracer than Ni isotopes that showed isotope fractionation during the smelting process (Ratié et al., 2016).

Finally, a review published by Warner et al. (2006) has shown similar concentration results during different steps of the Ni RKEF smelting processes throughout the world (the Dominican Republic,

Colombia, Venezuela, Brazil, Japan, New Caledonia, Indonesia, Ukraine, Macedonia and Greece). The feeding material from Barro Alto exhibits means concentration values of 2 wt% of Ni and 15.3 wt% of Fe (n = 13, Ratié et al., 2016), whereas the global average is 1.9 ± 0.5 wt% and 17 ± 5 wt%, respectively. The total average Fe content in slag material is 10 wt% at Barro Alto, whereas in the global mean value is 15 ± 10 wt%. The feeding material composition and the main wastes are therefore similar for the Barro Alto smelter and the global laterite Ni smelters. Moreover, the calcination, smelting and refining temperatures used are similar for the Barro Alto plant (850°C, 1,600°C and 1,550°C, respectively) and the other cited RKEF smelters (880 ± 120°C, n=13; 1,570 ± 35°C, n = 12; 1,440 ± 120°C, n = 10, respectively). This comparison suggests that the behavior of the Fe isotope system during pyrometallurgical processing at the Barro Alto plant is likely applicable to other plants elsewhere in the world.

4. Conclusions

For the first time, this study shows the Fe isotope composition for the complete series of natural and anthropogenic processes in the Barro Alto ultramafic complex. No significant Fe isotope variations were identified in either the pedogenesis of lateritic soils or the pyrometallurgical processes of Ni ore refining. The δ^{57}Fe value of the protolith fell within the range of the Fe isotope composition of the bulk silicate Earth, which is estimated at approximately 0.1 ‰ (Poitrasson, 2006), and is similar to deep lateritic profiles studied elsewhere. In the Ni laterite RKEF smelting process at Barro Alto, the rapid equilibrium of Fe isotopes between the different phases composing the FeNi ore melt at 1,600°C in the electric furnace results in undetectable Fe isotopic fractionation. This mechanism is supported by laboratory experiments under controlled conditions with high pressure and temperature equilibration between FeNi alloys and ultramafic silicate melts (Poitrasson et al., 2009).

As a consequence, the δ^{57}Fe values obtained from both pedogenesis (protolith to topsoil) and pyrometallurgical samples are homogeneous and may challenge the discrimination of anthropic and natural sources. Further studies should verify the potential fractionation induced by postdepositional processes as

demonstrated for Ni (Ratié et al., 2016) and Zn (Yin et al., 2018). Nonetheless, the conservation of the $\delta^{57}Fe$ values from the ores to the byproducts is an advantage for tracing anthropogenic sources when (i) the pyrometallurgical plant uses feeding material with Fe ores imported from other geological unities exhibiting different $\delta^{57}Fe$ values and/or (ii) the byproducts are transported or dispersed to other locations with different $\delta^{57}Fe$ values in the topsoil. In these cases, Fe isotopes could be a more suitable environmental tracer of anthropogenic sources than Ni isotopes.

Acknowledgments

We express our sincere thanks to the Anglo American staff at the Barro Alto mine (Goiás, Brazil). The authors acknowledge Gael Monvoisin for maintaining the GEOPS clean laboratory facilities and J. Chmeleff from the GET laboratory (Toulouse, France) for maintaining the MC ICP MS in good working order. The analytical work in Toulouse along with travel by JG and LCV was partly funded by the LMI-OCE and the 7th European Community Framework Program (NIDYFICS, n°318123) and the CLIM-AMAZON laboratory (INCO-LAB grant n°295091). The analytical work in Brazil and France was partly funded by the LMI-OCE and CNPq 445423/2014-5, 400029/2015-4 and 420697/2018-7. Gildas acknowledges the Faculty of Environmental Sciences, Czech University of Life Sciences, Prague (Grant n° 42900/1312/3166), the Czech Science Foundation 18-07585S, the French Ministry of National Education and Research (G. Ratié PhD grant), CAPES and the CNPq for support during his PhD. Jérémie Garnier was supported by CNPq grant 302722/2018-1. Daniel F. Araújo thanks the POLLUSOLS project framework and Ifremer (Centre Atlantique) for the financial support.

References

Anglo American PLC Annual Report, 2012, 2012.

Anglo American PLC Annual Report, 2017, 2017.

Anglo American PLC Annual Report, 2018, 2018.

Akerman, A., Poitrasson, F., Oliva, P., Audry, S., Prunier, J., Braun, J.J., 2014. Isotopic fingerprint of Fe cycling in an equatorial soil-plant-water system: The Nsimi watershed, South Cameroon. Chemical Geology, 385: 104-116.

Araújo, D.F., Ponzevera, E., Briant, N., Knoery, J., Sireau, T., Mojtahid, M., Metzger, E., Brach-Papa, C., 2019a. Assessment of the metal contamination evolution in the Loire estuary using Cu and Zn stable isotopes and geochemical data in sediments. Mar. Pollut. Bull. 143, 12–23.

Araújo, D. F., Ponzevera, E., Briant, N., Knoery, J., Bruzac, S., Sireau, T., Brach-Papa, C.,2019b. Copper, zinc and lead isotope signatures of sediments from a mediterranean coastal bay impacted by naval activities and urban sources. Applied Geochemistry, 111, 104440.

Barna, R., Moszkowicz, P., Gervais, C., 2004. Leaching assessment of road materials containing primary lead and zinc slags. Waste Manag. 24, 945–955.

Beard, B.L., Handler, R.M., Scherer, M.M., Wu, L., Czaja, A.D., Heimann, A., Johnson, C.M., 2010. Iron isotope fractionation between aqueous ferrous iron and goethite. Earth Planet. Sci. Lett. 295, 241–250.

Bigalke, M., Weyer, S., Kobza, J., & Wilcke, W., 2010. Stable Cu and Zn isotope ratios as tracers of sources and transport of Cu and Zn in contaminated soil. Geochimica et Cosmochimica Acta, 74(23), 6801-6813.

Borrok, D.M., Wanty, R.B., Ridley, W.I., Lamothe, P.J., Kimball, B.A., Verplanck, P.L., Runkel, R.L., 2009. Application of iron and zinc isotopes to track the sources and mechanisms of metal loading in a mountain watershed. Appl. Geochem. 24, 1270–1277. https://doi.org/10.1016/j.apgeochem.2009.03.010

Bril, H., Zainoun, K., Puziewicz, J., Courtin-Nomade, A., Vanaecker, M., Bollinger, J.-C., 2008. Secondary phases from the alteration of a pile of zinc-smelting slag as indicators of environmental conditions: An example from Swietochłowice, Upper Silesia, Poland. Can. Mineral. 46, 1235–1248.

Bullen, T.D., 2014. 7.10 - Metal Stable Isotopes in Weathering and Hydrology, in: Holland, H.D., Turekian, K.K. (Eds.), Treatise on Geochemistry (Second Edition). Elsevier, Oxford, pp. 329–359.

Butt, C.R., Cluzel, D., 2013. Nickel laterite ore deposits: weathered serpentinites. Elements 9, 123–128.

Chen, J. B., Busigny, V., Gaillardet, J., Louvat, P., & Wang, Y. N. (2014). Iron isotopes in the Seine River (France): Natural versus anthropogenic sources. Geochimica et Cosmochimica Acta, 128, 128-143.

Cheng, Y.B., Mao, J.W., Zhu, X.K., Wang, Y., 2015. Iron isotope fractionation during supergene weathering process and its application to constrain ore genesis in Gaosong deposit, Gejiu district, SW China. Gondwana Research, 27(3): 1283-1291.

Chrastný, V., Čadková, E., Vaněk, A., Teper, L., Cabala, J., Komárek, M., 2015. Cadmium isotope fractionation within the soil profile complicates source identification in relation to Pb–Zn mining and smelting processes. Chem. Geol. 405, 1–9. https://doi.org/10.1016/j.chemgeo.2015.04.002

Colin, F., Nahon, D., Trescases, J. J., & Melfi, A. J. (1990). Lateritic weathering of pyroxenites at Niquelandia, Goias, Brazil; the supergene behavior of nickel. Economic Geology, 85(5), 1010-1023.

Conway, T.M., Hamilton, D.S., Shelley, R.U., Aguilar-Islas, A.M., Landing, W.M., Mahowald, N.M., John, S.G., 2019. Tracing and constraining anthropogenic aerosol iron fluxes to the North Atlantic Ocean using iron isotopes. Nat. Commun. 10, 1–10.

Crundwell, F.K., Moats, M.S., Ramachandran, V., Robinson, T.G., Davenport, W.G., 2011. Chapter 7 - Refining Molten Ferronickel, in: Davenport, F.K.C.S.M.R.G.R.G. (Ed.), Extractive Metallurgy of Nickel, Cobalt and Platinum Group Metals. Elsevier, Oxford, pp. 85–93.

Dalvi, A.D., Bacon, W.G., Osborne, R.C., 2004. Past and future of nickel laterite projects.

Dauphas, N., John, S.G., Rouxel, O., 2017. Iron isotope systematics. Rev. Mineral. Geochem. 82, 415–510.

De Oliveira, S. B., Trescases, J. J., & Melfi, A. J. (1992). Lateritic nickel deposits of Brazil. Mineralium deposita, 27(2), 137-146.

Dublet, G., Juillot, F., Morin, G., Fritsch, E., Fandeur, D., Brown, G.E., 2015. Goethite aging explains Ni depletion in upper units of ultramafic lateritic ores from New Caledonia. Geochim. Cosmochim. Acta 160, 1–15. https://doi.org/10.1016/j.gca.2015.03.015

Dublet, G., Juillot, F., Morin, G., Fritsch, E., Fandeur, D., Ona-Nguema, G., Brown, G.E., 2012. Ni speciation in a New Caledonian lateritic regolith: A quantitative X-ray absorption spectroscopy investigation. Geochim. Cosmochim. Acta 95, 119–133.

Emmanuel, S., Erel, Y., Matthews, A., Teutsch, N., 2005. A preliminary mixing model for Fe isotopes in soils. Chem. Geol. 222, 23–34.

Ettler, V., Johan, Z., 2014. 12 years of leaching of contaminants from Pb smelter slags: Geochemical/mineralogical controls and slag recycling potential. Appl. Geochem. 40, 97–103.

Ettler, V., Kvapil, J., Šebek, O., Johan, Z., Mihaljevič, M., Ratié, G., Garnier, J., Quantin, C., 2016. Leaching behaviour of slag and fly ash from laterite nickel ore smelting (Niquelândia, Brazil). Appl. Geochem. 64, 118–127.

Ettler, V., Polák, L., Mihaljevič, M., Ratié, G., Garnier, J., Quantin, C., 2018. Oral bioaccessibility of inorganic contaminants in waste dusts generated by laterite Ni ore smelting. Environ. Geochem. Health 40, 1699–1712.

Fabre, S., Nedelec, A., Poitrasson, F., Strauss, H., Thomazo, C., Nogueira, A., 2011. Iron and sulphur isotopes from the Carajas mining province (Para, Brazil): Implications for the oxidation of the ocean and the atmosphere across the Archaean-Proterozoic transition. Chemical Geology, 289(1-2): 124-139.

Fantle, M.S., DePaolo, D.J., 2004. Iron isotopic fractionation during continental weathering. Earth Planet. Sci. Lett. 228, 547–562.

Fekiacova, Z., Pichat, S., Cornu, S., Balesdent, J., 2013. Inferences from the vertical distribution of Fe isotopic compositions on pedogenetic processes in soils. Geoderma, 209: 110-118.

Ferreira Filho, C.F., Pimentel, M.M., de Araujo, S.M., Laux, J.H., 2010. Layered intrusions and volcanic sequences in Central Brazil: geological and geochronological constraints for Mesoproterozoic (1.25 Ga) and Neoproterozoic (0.79 Ga) igneous associations. Precambrian Res. 183, 617–634.

Flament, P., Mattielli, N., Aimoz, L., Choel, M., Deboudt, K., de Jong, J., Rimetz-Planchon, J., Weis, D., 2008. Iron isotopic fractionation in industrial emissions and urban aerosols. Chemosphere 73, 1793–1798. https://doi.org/10.1016/j.chemosphere.2008.08.042

Gall, L., Williams, H.M., Halliday, A.N., Kerr, A.C., 2017. Nickel isotopic composition of the mantle. Geochim. Cosmochim. Acta 199, 196–209. https://doi.org/10.1016/j.gca.2016.11.016

Ganne, P., Cappuyns, V., Vervoort, A., Buvé, L., Swennen, R., 2006. Leachability of heavy metals and arsenic from slags of metal extraction industry at Angleur (eastern Belgium). Sci. Total Environ. 356, 69–85. https://doi.org/10.1016/j.scitotenv.2005.03.022

Ginoza, M., March, N.H., 1985. Isotope Effects in Liquid Metals. Phys. Chem. Liq. 15, 75–111. https://doi.org/10.1080/00319108508078471

Graham, S., Pearson, N., Jackson, S., Griffin, W., O'Reilly, S.Y., 2004. Tracing Cu and Fe from source to porphyry: in situ determination of Cu and Fe isotope ratios in sulfides from the Gratsberg Cu-Au deposit. Chemical Geology, 207: 147-169.

Herbert Jr, R.B., Schippers, A., 2008. Iron isotope fractionation by biogeochemical processes in mine tailings. Environ. Sci. Technol. 42, 1117–1122.

Houben, D., Couder, E., Sonnet, P., 2013. Leachability of cadmium, lead, and zinc in a long-term spontaneously revegetated slag heap: implications for phytostabilization. J. Soils Sediments 13, 543–554.

Johnson, C.M., Beard, B.L., 2006. Fe isotopes: an emerging technique for understanding modern and ancient biogeochemical cycles. GSA TODAY 16, 4.

Johnson, C. M., Beard, B. L., & Roden, E. E., 2008. The iron isotope fingerprints of redox and biogeochemical cycling in modern and ancient Earth. Annu. Rev. Earth Planet. Sci., 36, 457-493.

Kavner, A., John, S.G., Sass, S., Boyle, E.A., 2008. Redox-driven stable isotope fractionation in transition metals: Application to Zn electroplating. Geochim. Cosmochim. Acta 72, 1731–1741.

Klein, S., & Rose, T. (2020). Evaluating copper isotope fractionation in the metallurgical operational chain: An experimental approach. Archaeometry.

Kurisu, M., Takahashi, Y., Iizuka, T., Uematsu, M., 2016. Very low isotope ratio of iron in fine aerosols related to its contribution to the surface ocean. J. Geophys. Res. Atmospheres 121, 11,119-11,136.

Li, M., He, Y.S., Kang, J.T., Yang, X.Y., He, Z.W., Yu, H.M., Huang, F., 2017. Why was iron lost without significant isotope fractionation during the lateritic process in tropical environments? Geoderma, 290: 1-9.

Liu, S.A., Teng, F.Z., Li, S.G., Wei, G.J., Ma, J.L., Li, D.D., 2014. Copper and iron isotope fractionation during weathering and pedogenesis: Insights from saprolite profiles. Geochimica Et Cosmochimica Acta, 146: 59-75.

Lodding, A., Mundy, J.N., Ott, A., 1970. Isotope Inter-Diffusion and Self-Diffusion in Solid Lithium Metal. Phys. Status Solidi B 38, 559–569. https://doi.org/10.1002/pssb.19700380206

Manceau, A., Schlegel, M.L., Musso, M., Sole, V.A., Gauthier, C., Petit, P.E., Trolard, F., 2000. Crystal chemistry of trace elements in natural and synthetic goethite. Geochim. Cosmochim. Acta 64, 3643–3661.

Markl, G., von Blanckenburg, F., Wagner, T., 2006. Iron isotope fractionation during hydrothermal ore deposition and alteration. Geochimica Et Cosmochimica Acta, 70(12): 3011-3030.

Mattielli, N., Rimetz, J., Petit, J., Perdrix, E., Deboudt, K., Flament, P., Weis, D., 2006. Zn Cu isotopic study and speciation of airborne metal particles within a 5-km zone of a lead/zinc smelter. Geochim. Cosmochim. Acta Suppl. 70, A401–A401.

Milot, J., Poitrasson, F., Baron, S., Coustures, M.-P., 2016. Iron isotopes as a potential tool for ancient iron metals tracing. J. Archaeol. Sci. 76, 9–20.

Milot, J., Baron, S., Poitrasson, F., 2018. Potential use of Fe isotopes for ancient non-ferrous metals tracing through the example of a lead-silver production site (Imiter miner, Anti-Atlas, Morocco). Journal of Archaeological Science, 98: 22-33.

Moore, P. (2012). Anglo's new nickel. International Mining, March, 20-24.

Navarro, A., Cardellach, E., Mendoza, J.L., Corbella, M., Domènech, L.M., 2008. Metal mobilization from base-metal smelting slag dumps in Sierra Almagrera (Almería, Spain). Appl. Geochem. 23, 895–913. https://doi.org/10.1016/j.apgeochem.2007.07.012

Nriagu, J., Pacyna, J., 1988. Quantitative assesment of worldwide contamination of air, water and soils by trace-metals. Nature 333, 134–139. https://doi.org/10.1038/333134a0

Ott, A., 1969. Isotope Separation by Thermal Diffusion in Liquid Metal. Science 164, 297–297. https://doi.org/10.1126/science.164.3877.297

Oxley, A., Smith, M.E., Caceres, O., 2016. Why heap leach nickel laterites? Miner. Eng. 88, 53–60.

Pi, Q.H., Zhong, R.C., Hu, R.Z., 2015. Tracing the ore-formation history of the shear-zone-controlled Huogeqi Cu-Pb-Zn deposit in Inner Mongolia, northern China, using H, O, S, and Fe isotopes. Ore Geology Reviews, 71: 263-272.

Platzner, I. T., 1997. Modern isotope ratio mass spectrometry. Wiley, Chichester, p 514.

Poitrasson, F., 2006. On the iron isotope homogeneity level of the continental crust. Chem. Geol. 235, 195–200. https://doi.org/10.1016/j.chemgeo.2006.06.010

Poitrasson, F., Freydier, R., 2005. Heavy iron isotope composition of granites determined by high resolution MC-ICP-MS. Chem. Geol. 222, 132–147. https://doi.org/10.1016/j.chemgeo.2005.07.005

Poitrasson, F., Roskosz, M., Corgne, A., 2009. No iron isotope fractionation between molten alloys and silicate melt to 2000 °C and 7.7 GPa: Experimental evidence and implications for planetary differentiation and accretion. Earth Planet. Sci. Lett. 278, 376–385. https://doi.org/10.1016/j.epsl.2008.12.025

Poitrasson, F., Vieira, L.C., Seyler, P., dos Santos Pinheiro, G.M., Mulholland, D.S., Bonnet, M.-P., Martinez, J.-M., Lima, B.A., Boaventura, G.R., Chmeleff, J., 2014. Iron isotope composition of the bulk waters and sediments from the Amazon River Basin. Chem. Geol. 377, 1–11.

Poitrasson, F., Viers, J., Martin, F., Braun, J.-J., 2008. Limited iron isotope variations in recent lateritic soils from Nsimi, Cameroon: implications for the global Fe geochemical cycle. Chem. Geol. 253, 54–63.

Quantin, C., Becquer, T., Rouiller, J.H., Berthelin, J., 2002. Redistribution of metals in a New Caledonia ferralsol after microbial weathering. Soil Sci. Soc. Am. J. 66, 1797–1804.

Ratié, G., Garnier, J., Calmels, D., Vantelon, D., Guimarães, E., Monvoisin, G., Nouet, J., Ponzevera, E., Quantin, C., 2018. Nickel distribution and isotopic fractionation in a Brazilian lateritic regolith: Coupling Ni isotopes and Ni K-edge XANES. Geochim. Cosmochim. Acta 230, 137–154.

Ratié, G., Jouvin, D., Garnier, J., Rouxel, O., Miska, S., Guimarães, E., Cruz Vieira, L., Sivry, Y., Zelano, I., Montarges-Pelletier, E., Thil, F., Quantin, C., 2015. Nickel isotope fractionation during tropical weathering of ultramafic rocks. Chem. Geol. 402, 68–76. https://doi.org/10.1016/j.chemgeo.2015.02.039

Ratié, G., Quantin, C., Jouvin, D., Calmels, D., Ettler, V., Sivry, Y., Vieira, L.C., Ponzevera, E., Garnier, J., 2016. Nickel isotope fractionation during laterite Ni ore smelting and refining: Implications for tracing the sources of Ni in smelter-affected soils. Appl. Geochem. 64, 136–145.

Rauch, J.N., Pacyna, J.M., 2009. Earth's global Ag, Al, Cr, Cu, Fe, Ni, Pb, and Zn cycles. Glob. Biogeochem. Cycles 23, GB2001. https://doi.org/10.1029/2008GB003376

Seignez, N., Gauthier, A., Bulteel, D., Damidot, D., Potdevin, J.-L., 2008. Leaching of lead metallurgical slags and pollutant mobility far from equilibrium conditions. Appl. Geochem. 23, 3699–3711. https://doi.org/10.1016/j.apgeochem.2008.09.009

Shiel, A.E., Weis, D., Orians, K.J., 2010. Evaluation of zinc, cadmium and lead isotope fractionation during smelting and refining. Sci. Total Environ. 408, 2357–2368. https://doi.org/10.1016/j.scitotenv.2010.02.016

Šillerová, H., Chrastný, V., Vítková, M., Francová, A., Jehlička, J., Gutsch, M.R., Kocourková, J., Aspholm, P.E., Nilsson, L.O., Berglen, T.F., 2017. Stable isotope tracing of Ni and Cu pollution in North-East Norway: Potentials and drawbacks. Environ. Pollut. 228, 149–157.

Sivry, Y., Riotte, J., Sonke, J.E., Audry, S., Schäfer, J., Viers, J., Blanc, G., Freydier, R., Dupré, B., 2008. Zn isotopes as tracers of anthropogenic pollution from Zn-ore smelters The Riou Mort–Lot River system. Chem. Geol. 255, 295–304.

Sonke, J.E., Sivry, Y., Viers, J., Freydier, R., Dejonghe, L., Andre, L., Aggarwal, J.K., Fontan, F., Dupre, B., 2008. Historical variations in the isotopic composition of atmospheric zinc deposition from a zinc smelter. Chem. Geol. 252, 145–157. https://doi.org/10.1016/j.chemgeo.2008.02.006

Souto-Oliveira, C.E., Babinski, M., Araújo, D.F., Andrade, M.F., 2018. Multi-isotopic fingerprints (Pb, Zn, Cu) applied for urban aerosol source apportionment and discrimination. Sci. Total Environ. 626, 1350–1366.

Souto-Oliveira, C.E., Babinski, M., Araújo, D.F., Weiss, D.J., Ruiz, I.R., 2019. Multi-isotope approach of Pb, Cu and Zn in urban aerosols and anthropogenic sources improves tracing of the atmospheric pollutant sources in megacities. Atmos. Environ. 198, 427–437.

Teixeira, N.L., Caxito, F.A., Rosière, C.A., Pecoits, E., Vieira, L.C., Frei, R., Sial, A.N., Poitrasson, F., 2017. Trace elements and isotope geochemistry (C, O, Fe, Cr) of the Cauê iron formation, Quadrilatero Ferrifero, Brazil: Evidence for widespread microbial dissimilatory iron reduction at the Archean/Proterozoic transition. Precambrian Research, 298: 39-55.

Thompson, A., Ruiz, J., Chadwick, O.A., Titus, M., Chorover, J., 2007. Rayleigh fractionation of iron isotopes during pedogenesis along a climate sequence of Hawaiian basalt. Chem. Geol. 238, 72–83.

Wang, Y., Zhu, X.K., Mao, J.W., Li, Z.H., Cheng, Y.B., 2011. Iron isotope fractionation during skarn-type metallogeny: A case study of Xinqiao Cu-S-Fe-Au deposit in the Middle-Lower Yangtze valley. Ore Geology Reviews, 43(1): 194-202.

Warner, A.E.M., Diaz, C.M., Dalvi, A.D., Mackey, P.J., Tarasov, A.V., 2006. JOM world nonferrous smelter survey, part III: Nickel: Laterite. Jom 58, 11–20.

Wasylenki, L. E., Howe, H. D., Spivak-Birndorf, L. J., & Bish, D. L. (2015). Ni isotope fractionation during sorption to ferrihydrite: implications for Ni in banded iron formations. Chemical Geology, 400, 56-64.

Wawryk, C.M., Foden, J.D., 2015. Fe-isotope fractionation in magmatic-hydrothermal mineral deposits: A case study from the Renison Sn-W deposit, Tasmania. Geochimica et Cosmochimica Acta, 150: 285-298.

Wiederhold, J.G., 2015. Metal Stable Isotope Signatures as Tracers in Environmental Geochemistry. Environ. Sci. Technol. 49, 2606–2624. https://doi.org/10.1021/es504683e

Wiederhold, J.G., Teutsch, N., Kraemer, S.M., Halliday, A.N., Kretzschmar, R., 2007. Iron isotope fractionation in oxic soils by mineral weathering and podzolization. Geochim. Cosmochim. Acta 71, 5821–5833.

Wu, B., Amelung, W., Xing, Y., Bol, R., & Berns, A. E., 2019. Iron cycling and isotope fractionation in terrestrial ecosystems. Earth-science reviews, 190, 323-352.

Yamaguchi, K.E., Johnson, C.M., Beard, B.L., Beukes, N.J., Gutzmer, J., Ohmoto, H., 2007. Isotopic evidence for iron mobilization during Paleoproterozoic lateritization of the Hekpoort paleosol profile from Gaborone, Botswana. Earth Planet. Sci. Lett. 256, 577–587.

Yin, N.-H., van Hullebusch, E.D., Benedetti, M., Lens, P.N.L., Sivry, Y., 2018. Zn isotopes fractionation during slags' weathering: One source of contamination, multiple isotopic signatures. Chemosphere 195, 483–490. https://doi.org/10.1016/j.chemosphere.2017.11.184.

Table captions

Table 1: List of natural and pyrometallurgical samples and their Fe and Zr contents. $\tau_{Fe} = ([Fe]/[Zr]_{sample}/[Fe]/[Zr]_{protolith} -1)$, where the sample RC 27-28 represents the protolith. The Fe isotope composition and two standard errors are calculated from the 3 analyses using Student's t-corrected factor (Platzner, 1997). δFe/amu is the deviation of the Fe isotope composition of a sample relative to the standard and normalized to a mass difference of 1 atomic mass unit (amu).

Sample name	Depth	[Fe]	[Zr]	τ_{Fe}	$\delta^{57}Fe$		2 SE	δFe/amu
		g kg^{-1}	*mg kg^{-1}*		*‰*			
By products								
Ore 1		165			0.00	±	0.18	0.00
Ore 5		118			0.03	±	0.20	0.01
SS7		106			-0.10	±	0.09	-0.03
SS8		124			0.05	±	0.14	0.02
WRS		71			0.07	±	0.08	0.02
BRS		179			0.05	±	0.11	0.02
FeNi2		689			0.07	±	0.12	0.02
Soil samples								
BAS1 0-10	0-10 cm	271	14	-0.10	-0.10	±	0.07	-0.03
BAS1 10-30	10-30 cm	261	13	-0.09	0.02	±	0.15	0.01
BAS1 30-80	30-80 cm	255	13	-0.08	0.00	±	0.13	0.00
Lateritic samples								
RC0-1	3-4 m	256	11	0.08	0.07	±	0.05	0.02
RC6-7	9-10 m	369	14	0.22	-0.06	±	0.11	-0.02
RC16-17	19-20 m	85	4	0.01	0.02	±	0.19	0.01
RC24-25	27-28 m	67	3	0.05	0.02	±	0.34	0.01
RC27-28	30-31 m	49	2	0.00	0.08	±	0.20	0.03

Figure captions

Figure 1: Schematic view of the FeNi smelting and refining processes modified from Ettler et al. (2016) showing the average Ni and Fe contents in ore (n= 7), F (n=10), SS (n=8), WRS (n=1), BRS (n=1) and FeNi (n=2) (Ratié et al., 2016).

Figure 2: Iron isotopic values (δ^{57}Fe in ‰) vs. the τ_{Fe} normalized by Zr (Poitrasson et al., 2008; our study), Th (Liu et al., 2014) and Ti (Li et al., 2017). The vertical black line represents the border between the gain and loss of Fe. The blue band represents the δ^{57}Fe value of the bulk silicate Earth (Poitrasson et al., 2006). Error bars represent 2 SD (Liu et al., 2014; Li et al., 2017) and 2 SE (Poitrasson et al., 2008; our study).

Figure 3: δNi/amu and δFe/amu values for lateritic profile, ultramafic (UM) soils and products from mining (feed material) and smelting (smelting slags, refining slags, and FeNi) activities. δNi/amu values were calculated based on the $\delta^{60/58}$Ni values in Ratié et al. (2015, 2016, 2018). The green band represents the δNi/amu value of the bulk silicate Earth (Gall et al., 2017) and the blue band represents the δFe/amu value of the bulk silicate Earth (Poitrasson, 2006). The dotted line separates anthropogenic samples from geogenic samples.

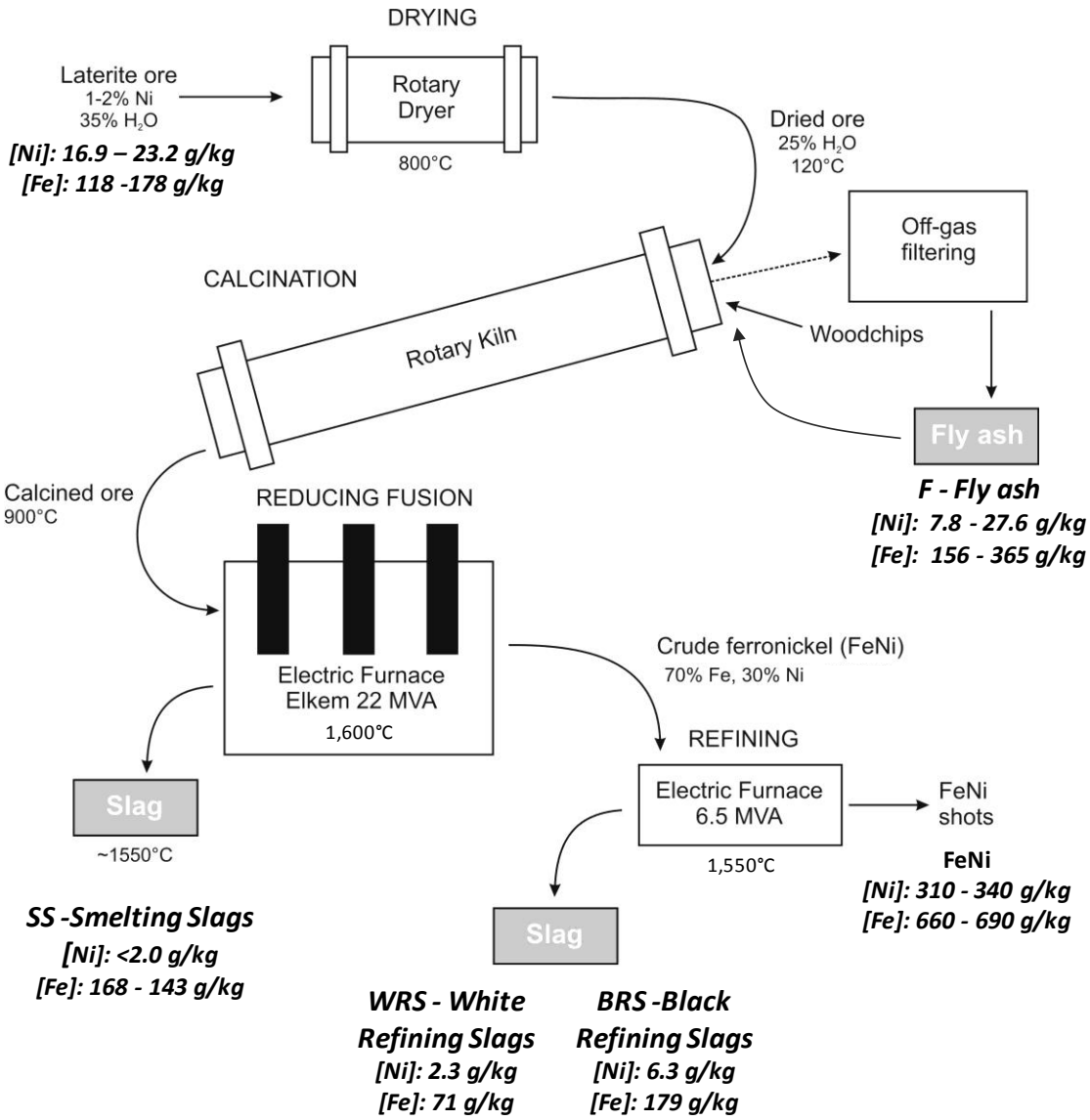
DRYING
Laterite ore
1-2% Ni
35% H2O
[Ni]: 16.9 – 23.2 g/kg
[Fe]: 118 -178 g/kg
Rotary Dryer
800°C
Dried ore
25% H2O
120°C
Off-gas filtering
CALCINATION
Rotary Kiln
Woodchips
Fly ash
F - Fly ash
[Ni]: 7.8 - 27.6 g/kg
[Fe]: 156 - 365 g/kg
Calcined ore
900°C
REDUCING FUSION
Electric Furnace
Elkem 22 MVA
1,600°C
Crude ferronickel (FeNi)
70% Fe, 30% Ni
REFINING
Electric Furnace
6.5 MVA
1,550°C
FeNi shots
FeNi
[Ni]: 310 - 340 g/kg
[Fe]: 660 - 690 g/kg
Slag
~1550°C
SS -Smelting Slags
[Ni]: <2.0 g/kg
[Fe]: 168 - 143 g/kg
Slag
WRS - White Refining Slags
[Ni]: 2.3 g/kg
[Fe]: 71 g/kg
BRS -Black Refining Slags
[Ni]: 6.3 g/kg
[Fe]: 179 g/kg

Figure 1

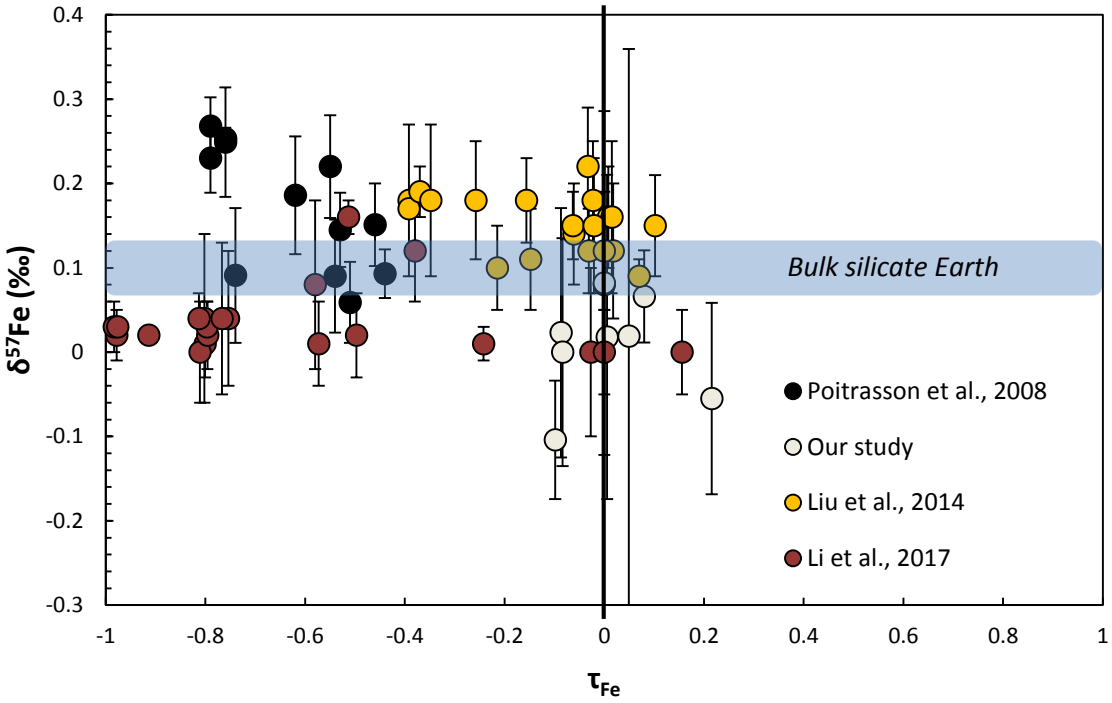
0.4
0.3
0.2
0.1
0
-0.1
-0.2
-0.3
δ57Fe (‰)
-1
-0.8
-0.6
-0.4
-0.2
0
0.2
0.4
0.6
0.8
1
τFe
Bulk silicate Earth
Poitrasson et al., 2008
Our study
Liu et al., 2014
Li et al., 2017

Figure 2

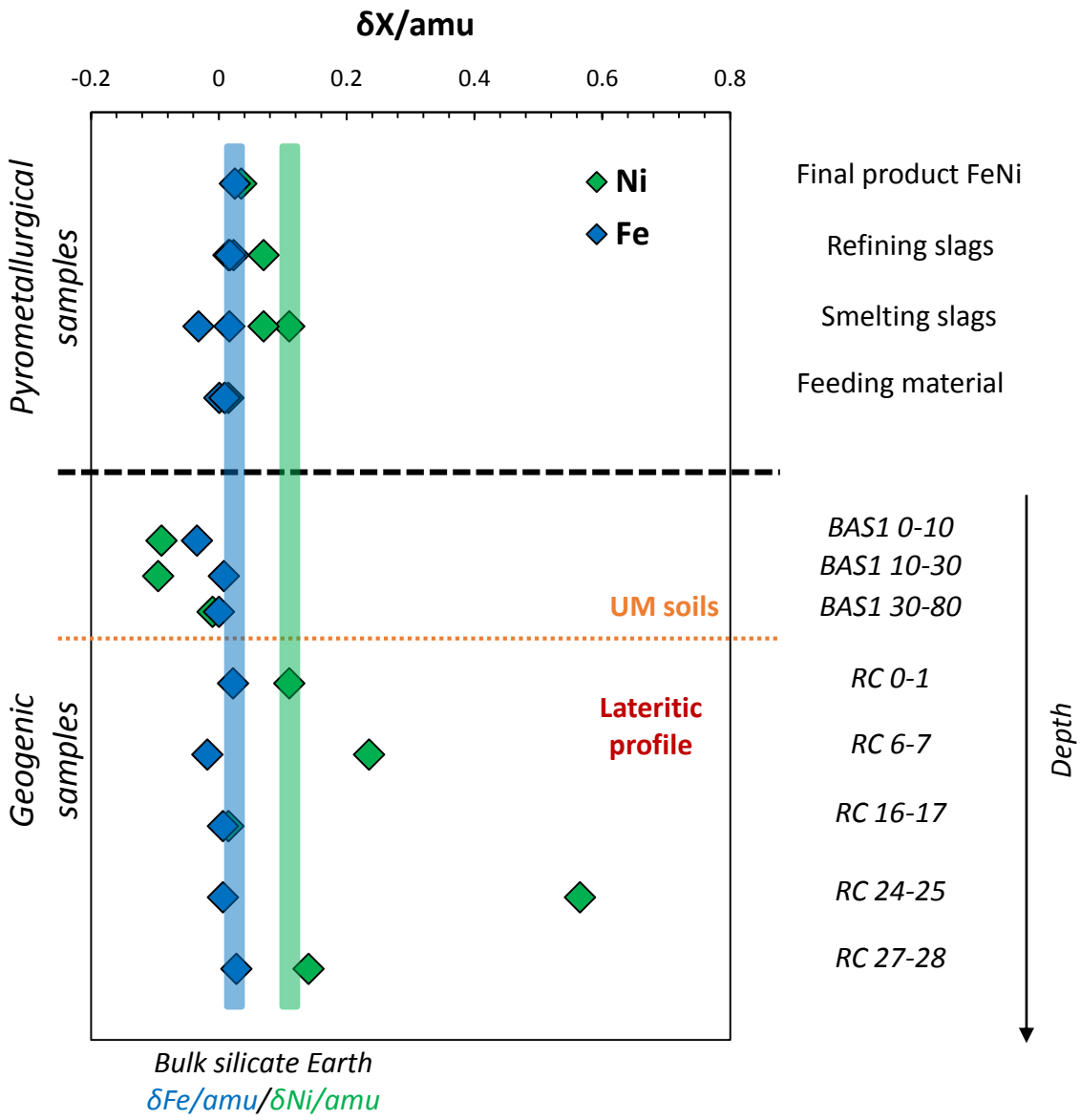
δX/amu
-0.2
0
0.2
0.4
0.6
0.8
Pyrometallurgical samples
Geogenic samples
Ni
Fe
Final product FeNi
Refining slags
Smelting slags
Feeding material
UM soils
Lateritic profile
BAS1 0-10
BAS1 10-30
BAS1 30-80
RC 0-1
RC 6-7
RC 16-17
RC 24-25
RC 27-28
Depth
Bulk silicate Earth
δFe/amu/δNi/amu

Figure 3